Research article

Death in the shallows: The record of Permo-Triassic mass extinction in paralic settings, southwest China

Paul B. Wignall[a,*], Daoliang Chu[b], Jason M. Hilton[c], Jacopo Dal Corso[a,b], Yuyang Wu[b], Yao Wang[b], Jed Atkinson[a], Jinnan Tong[b]

[a] School of Earth and Environment, University of Leeds, Leeds LS2 9JT, UK
[b] State Key Laboratory of Biogeology and Environmental Geology, School of Earth Sciences, China University of Geosciences, Wuhan 430074, China
[c] School of Geography, Earth and Environmental Sciences, University of Birmingham, Birmingham B15 2TT, UK

ABSTRACT

The Permo-Triassic marine mass extinction has been blamed on a range of culprits including anoxia, acidification, high temperature and increased sedimentation and nutrient influx, the last two being a direct consequence of terrestrial biomass die-off and climatic changes. In marine settings, the role of these kill mechanisms is likely to be depth-dependent with siltation and high temperatures potentially the most consequential in shallowest waters. These ideas have been investigated in a study of the Permo-Triassic boundary beds in western Guizhou and eastern Yunnan (WGEY) which record the transition from littoral coal swamps to an inner shelf/platform fringed by a coastal mudbelt. Anoxic conditions were not developed in such shallow waters but weak dysoxia is seen in the extinction interval, recorded by the presence of pyrite framboids and glauconite, and may have been a factor in the crisis even in coastal waters. High temperatures may also be an extinction factor as evidenced by the brief bloom of microgastropods in the immediate aftermath. The Late Permian peat-forming swamps were subject to considerable in situ erosion that reworked authigenic minerals (chamosite and kaolinite). This material, together with considerable amounts of charcoal, was concentrated in distinctive green sandstone beds. However, the notion that the marine extinction was caused by increased sediment supply, a death-by-siltation mechanism following the collapse of terrestrial biomass, is not supported by the field evidence because a surge in clastic influx onto the shelf is not observed during the extinction interval when a range of carbonates, including microbialites, developed. The sediment was likely trapped in alluvial plains during base-level rise and/or a short period of more arid conditions occurred, reducing the clastic supply in the coastal–shallow marine environments. Ocean acidification is another potent kill mechanism but the occurrence of the extinction within a transgressive, carbonate-dominated interval in the shallow-water locations of WGEY does not support this cause.

1. Introduction

The Permo-Triassic mass extinction (PTME) was the greatest crisis to afflict the biosphere, with severe losses ranging from the open ocean to the terrestrial realm (e.g. Yin et al., 2007; Wignall, 2015; Stanley, 2016). No ecosystem was left unscathed but it has been suggested that life in marginal marine settings, such as estuaries, may have fared better relative to other environments (Buatois et al., 2005; Zhang et al., 2017). Supporting evidence for this idea comes from the similar composition of both body and trace fossil assemblages from Permian and Triassic brackish settings which suggests that relatively few losses occurred at the erathem boundary in these environments (Briggs and Gall,

1990; Shu et al., 2018). Brackish faunas are usually subject to stressful conditions due to frequent and substantial salinity and temperature changes, which tends to favour opportunistic organisms with broad environmental tolerance (Buatois et al., 2005). Brackish fauna therefore has a pre-adaptation to high stresses that may have aided the preferential resilience and survival of coastal inhabitants during the PTME.

Anoxia, ocean acidification and high temperature have been highlighted as likely stress factors during the marine PTME (Wignall and Hallam, 1992; Benton and Twitchett, 2003; Payne et al., 2007; Joachimski et al., 2012; Sun et al., 2012; Song et al., 2014; Wignall, 2015) alongside dramatic increases of sediment influx (Sephton et al., 2005; Algeo and Twitchett, 2010; Benton and Newell, 2014; Kaiho

et al., 2016; Sun et al., 2018). Of these culprits, high temperatures and siltation may have been important factors for coastal communities because surface waters are generally the warmest part of the depth profile and sedimentation rates are highest adjacent to river mouths. In contrast, anoxia is likely to be more intense in deeper waters that are further removed from the mixed/oxygenated surface layers (Bond and Wignall, 2010; Song et al., 2014; Huang et al., 2017). Which if any of these factors were responsible for extinctions amongst the shallowest marine, latest Permian communities has yet to be directly examined using field evidence. Here we aim to investigate the palaeoenvironments during the PTME in the coastal sedimentary record of the Permian-Triassic transition in the western Guizhou – eastern Yunnan (WGEY) region and compare with the contemporary marine extinction losses. The region provides a series of outcrops that allows the study of a continuous transect from coastal mud-plains to shallow marine settings. The changing environments can therefore be "walked out" from land into shallow waters. Furthermore, the floral record of the WGEY region has already contributed substantially to our knowledge of the terrestrial PTME (Peng et al., 2005; Yu et al., 2007; Chu et al., 2016, 2020), which provides a rare chance to directly compare the relative timing of terrestrial and marine losses.

2. Materials and methods

Five sections and a cored borehole were measured in WGEY spanning the Permo-Triassic boundary interval (Fig. 1). Fossils, both marine invertebrate and plant, were observed and identified in the field. Selected beds were examined in thin section and polished blocks were studied using a scanning electron microscope (SEM): the latter approach allowed the pyrite content (where present) to be assessed and pyrite framboid diameters were measured. This parameter provides a

sensitive measure of oxygenation regimes ranging from dysoxic to euxinic conditions (for assessment technique see Bond and Wignall, 2010). Use of the SEM's electron microprobe facility also allowed the elemental composition (and thus the mineralogy) of the sedimentary phases to be assessed.

A total organic carbon isotope ($\delta^{13}C_{org}$) profile was generated for the Zhonghe section to help place the Permo-Triassic boundary at this location. Published isotopic records are already available for Chinahe and Zhongzhai (Zhang et al., 2014; Chu et al., 2020). Globally there is a major negative inflexion of $\delta^{13}C_{carb}$ values that begin in the latest Permian (*Clarkina changxingensis* Zone) and reach a low point in the *Clarkina yini* Zone. Values recover somewhat after this and are rising gently across the Permo-Triassic boundary (Shen et al., 2011). A major, negative carbon isotope excursion is also seen in the terrestrial organic carbon record around the Permo-Triassic boundary which therefore provides a valuable tool for correlation between the marine and terrestrial sphere (Wu et al., 2020).

For $\delta^{13}C_{org}$ analyses, ~2 g of powdered samples was reacted with 3 mol/L HCl for 24 h to remove carbonate, then rinsed with ultrapure water repeatedly until neutralized, and finally dried at 35 °C. The $\delta^{13}C_{org}$ values of the treated samples were obtained using an elemental analyser (EA) coupled with an isotope ratio mass spectrometer (Thermo Finnegan DeltaV) in the State Key Laboratory of Biogeology and Environmental Geology at the China University of Geosciences (Wuhan). The results were calibrated using USGS standards and the analytical precision of $\delta^{13}C_{org}$ was better than ± 0.2‰. $\delta^{13}C_{org}$ values are given in per mille relative to VPDB.

3. Regional geology and study sections

During the Permian and Triassic the WGEY region of South China
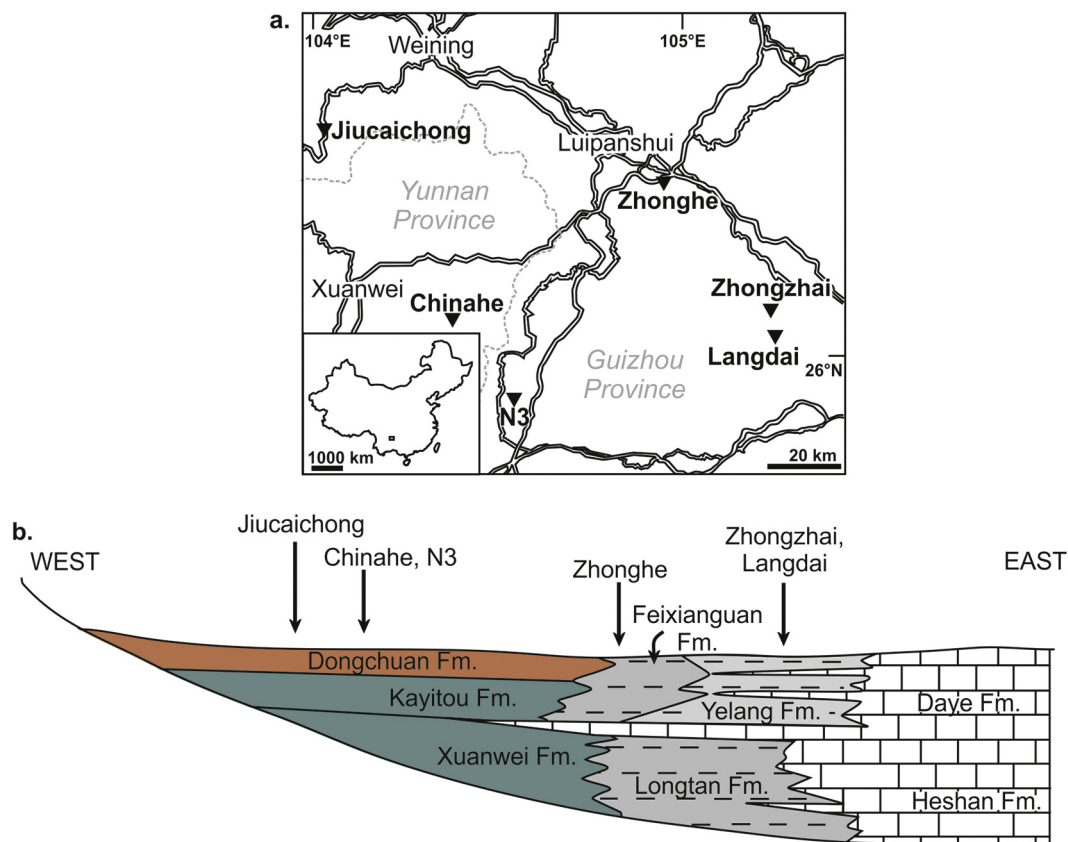
Fig. 1. Study area and stratigraphy in south-west China. (a). Location map of the western Guizhou-eastern Yunnan region of South China during the Permo-Triassic interval showing location of studied sections (from Chu et al., 2016), and (b) Schematic cross section of the Permo-Triassic formations, showing the location of the studied sections along this proximal-distal transect.

lay on the eastern margin of a landmass known as the Kangdian Oldland (Fig. 1a). In the Late Permian this was fringed by a belt of sandstones, mudstones and coals, that record coastal swamp and fluvial systems belonging to the Xuanwei Formation (Yu et al., 2007; Bercovici et al., 2015; Chu et al., 2016). These passed offshore into a mud-dominated, low energy shallow-marine mudstone facies belt around 100 km in width (Longtan Formation; Wang et al., 2011) before transitioning into platform carbonates of the Heshan Formation (Fig. 1b). The highest coal marks the top boundary of the Xuanwei Formation and the overlying Kayitou Formation is otherwise similar but lacks coals. Further eastwards the Kayitou Formation passes upwards into the Feixianguan Formation, a marine fine-clastic facies, interpreted to have formed in a broad lagoon (Bercovici et al., 2015), locally with thin beds of microbialite limestone in its basal part (described below). To the east of this the Feixianguan passes into a series of interbedded mudstones and limestone (Yelang Formation) which in turn passes into the limestones of the Daye Formation (Fig. 1b).

The position of the Permo-Triassic boundary in the terrestrial sections has been much debated: some have placed it near or at the top of the Xuanwei Formation (Bercovici et al., 2015), whilst Zhang et al. (2016) placed it much higher, at the top of the Kayitou Formation. The presence of Triassic-type marine bivalves and the Early Triassic conchostracan *Euestheria gutta* points to the boundary occurring in the lower-middle part of the Kayitou Formation (Chu et al., 2016; Song et al., 2019). A major extinction of the Permian flora is recorded in the basal part of the Kayitou Formation, a short distance above the topmost coal (Chu et al., 2016, 2020). The presence of a negative total organic carbon isotope excursion and a large mercury spike around the same level provide independent chemostratigraphic markers for the placement of the Permian-Triassic boundary immediately above this level (Chu et al., 2020).

Arranged in a proximal to distal order the study sections are:-.

3.1. Jiucaichong section

This hillside section near Jiucaichong village (Heishitou Town, Guizhou) exposes the contact between the sandstone, mudstone and coal beds of the Xuanwei Formation and the overlying Kayitou Formation which is dominated by grey-green mudstone in its lowest parts. Only the 3 *m* of strata straddling the formation boundary are studied here. The plant extinction has been studied in detail at this location: nine plant taxa are recorded of which two (*Lepidostrobophyllum megasporophylls* and *Stigmaria* roots) may have belonged to the same lycopsid plant species. The remaining plant fossils represent large-leaved plants from the Marattiales, gigantopterids and peltasperms. They occur immediately above the topmost coal but above this level only rare *Gigantopteris* leaves persist for a short interval, suggesting there was a sharp and severe floral extinction event in the basal-most Kayitou Formation (Chu et al., 2016).

3.2. Chinahe section

The Chinahe roadcut section is located in Tianba Town, Xuanwei City, eastern Yunnan Province. It exposes the same level as the Jiucaichong section and a similar range of lithologies although sandstone beds are more frequent in the Kayitou Formation as is the marine influence: bivalves, lingulid brachiopods and microgastropods appear 1.8 *m* above the base of the Formation and are present in the overlying 12 *m* of the unit (Song et al., 2019).

The plant record is known in detail at this location and reveals a similarly abrupt extinction to that seen at Jiucaichong (Chu et al., 2016, 2020). Often complete, large-leaved plants are common in the topmost metres of the Xuanwei Formation and have not experienced significant taphonomic fragmentation. These include a sphenopsid (*Lobatanularia cathaysiana*), marattialean ferns (vegetative leaves of *Pecopteris guizhouensis* and fertile leaves of *Rajhia guizhouensis*), the gigantopterid

Gigantonoclea sp. as well as *Stigmaria* (lycopsid roots). A further three species occur and persist (and are common) in the strata immediately above the topmost coal: the gigantopterids *Gigantopteris dictyophylloides* and *Gigantonocles guizhouensis* and *Pecopteris* sp. These taxa are typical of the Xuanwei Formation peat-forming community (He et al., 2019).

These abruptly disappear and are replaced by common *Peltaspermum* sp. and *Annalepis* sp.. The topmost coal marks the onset of a major decline in $\delta^{13}C_{org}$ values which fall from −25‰, reaching a lowpoint of −30‰, 3.7 *m* higher in the section (Chu et al., 2020). Correlation with the carbon isotope record at the GSSP (Meishan) suggests the disruption of the latest Permian flora in WGEY started before and culminated around the time that the main phase of marine extinctions began (Chu et al., 2020).

3.3. Borehole N3

This borehole was drilled in Panguan Town, Liupanshui City, western Guizhou Province. The entire Xuanwei Formation (235 *m* thick) was examined in a core and the petrography of the sandstone beds examined. These rest on basalts of the Emeishan large igneous province. The Xuanwei succession consists of numerous interbeds of sandstone, coal and mudstone that are typical of the Formation.

3.4. Zhonghe section

This hillside exposure in Guizhou Province reveals the uppermost limestone and mudstone beds of the Longtan Formation overlain by the maroon mudstones of the Feixianguan Formation. Thin limestone beds and thrombolite mounds are developed around the formation boundary.

3.5. Langdai sections

Two closely spaced roadcuts were examined. At one section, adjacent to the main road south of Langdai, a microbialite limestone was seen interbedded in a mudstone succession (Langdai-1). At the other roadcut (Langdai-2), approximately 200 *m* to the east and adjacent to a minor road, the limestone bed is missing and a mudstone-on-mudstone contact is developed that marks the formational boundary between the Longtan and Yelang formations (Fig. 1b). The macrofauna of the Longtan Formation is dominated by Permian brachiopods, especially chonetids, whilst the Yelang Formation contains a low diversity assemblage dominated by *Claraia*, a typical genus in the Early Triassic. These different faunas indicate that the Permo-Triassic boundary occurs at the formational boundary.

3.6. Zhongzhai section

This roadcut section is situated about 1 km northeast of Zhongzhai township in Liuzhi County of Guizhou. Despite being only a short distance from the Langdai sections (Fig. 1a), the Permo-Triassic boundary sediments are considerably different, with a metre thickness of limestone interleaved in the mudstone-dominated succession. Thus, the uppermost Longtan Formation consists of siltstone and limestone interbeds which are overlain by mudstone of the Feixianguan Formation (Metcalfe and Nicoll, 2007). The PTB boundary occurs within the limestones and their conodont biostratigraphy has received considerable attention. Nicoll and Metcalfe (2005) established a bed numbering scheme with the boundary beds numbered from 26 to 31. They placed the PTB at the base of Bed 30 based on the first occurrence of *Hindeodus parvus* at this level, and confirmed this finding in their later evaluation (Metcalfe and Nicoll, 2007). A subsequent conodont study by Zhang et al. (2014) confirmed that *H. parvus* becomes common at the base of Bed 30 but found rare examples of this species in Bed 28a, a horizon that otherwise yields Permian conodonts. Despite this finding, Zhang et al. (2014) continued to place the PTB at the base of Bed 30. The

$\delta^{13}C_{org}$ record from this section shows the distinct negative excursion seen globally (e.g. Schobben et al., 2019), although in more complete successions the excursion is seen to be composed of two lowpoints either side of the boundary (Xie et al., 2007; Yin et al., 2014). A single lowpoint in Bed 31 is seen at Bed 31 (Zhang et al., 2014). The abrupt 1‰ drop at the top of bed 29, and the absence of the first $\delta^{13}C_{org}$ minimum, suggests there is a hiatus at this level.

The Zhongzhai section has become substantially overgrown and obscured since these earlier studies, and only a short section (~40 cm thick), from beds 28a to 31, was excavated and studied in this work.

4. Sedimentology of the PTB beds

4.1. Jiucaichong section

Petrographic and microprobe analyses show that the green, medium-grained sandstone at the base of the measured section is composed predominantly of angular grains of chamosite and kaolinite with minor feldspar, quartz and rutile grains. This sandstone is overlain by two palaeosol and coal couplets; the former consist of siltstone with abundant rootlets. The highest coal marks the top of the Xuanwei Formation (Fig. 2). The overlying 25 cm-thick, grey-green mudstone bed at the base of the Kayitou Formation is organic rich and contains abundant Permian plants (cf. Chu et al., 2016). Microprobe analysis shows that kaolinite dominates the clay composition of this bed whilst small grains of phosphate are common in the mudstone. The overlying mudstone beds range from yellow to grey-green in colour and contain abundant mm-sized micronodules consisting of chamosite-chert intergrowths. Mudstone dominates the entire 15 m-thickness of the Kayitou Formation seen at Jiucaichong (Chu et al., 2016).

There is no evidence for marine influence in the Jiucaichong section (except perhaps for the presence of the small phosphate grains), and the coal and rootlet beds suggest a freshwater swamp setting during the PTB interval. Diagenetic chamosite and chert growth is ubiquitous and abundant in the Xuanwei Formation: Dai and Chou (2007) report that chamosite can form > 50% of the total mineral component of coals in this unit. The chamosite is considered to have formed from the interaction of kaolinite with Fe and Mg-rich fluids derived from the underlying Emeishan volcanic pile (Dai and Chou, 2007). The presence of the chamosite/chert micronodules in the overlying Kayitou mudstone beds indicates that these reaction products were not restricted to the Xuanwei coals but continued to form in the mudstones of the Kayitou Formation. Bercovici et al. (2015) interpret the mudstone at this location as a brackish, lagoonal facies but it lacks evidence for marine influence and is more likely a floodplain lake facies.

4.2. Chinahe section

The uppermost two metres of the Xuanwei Formation at Chinahe consist of interbeds of green sandstone and laminated siltstone with
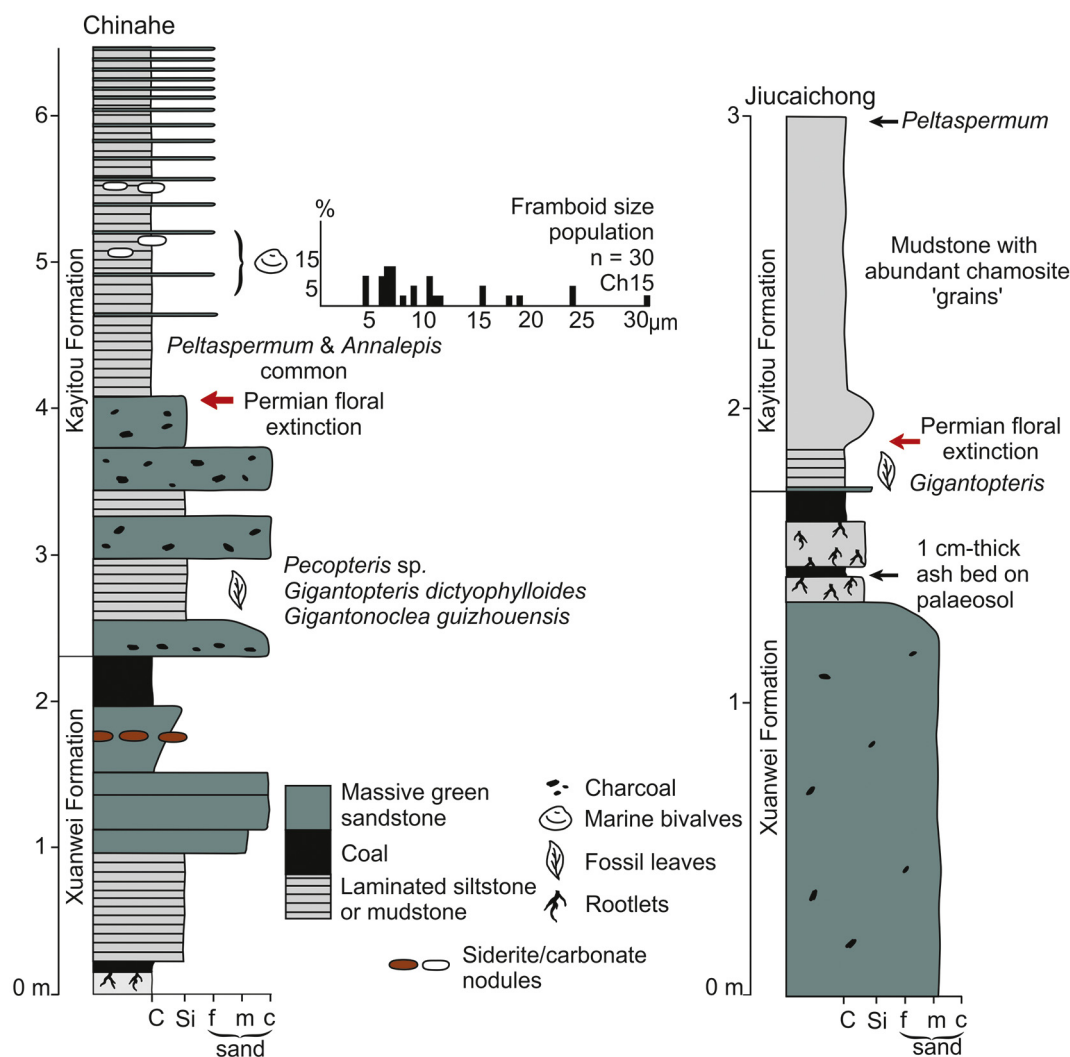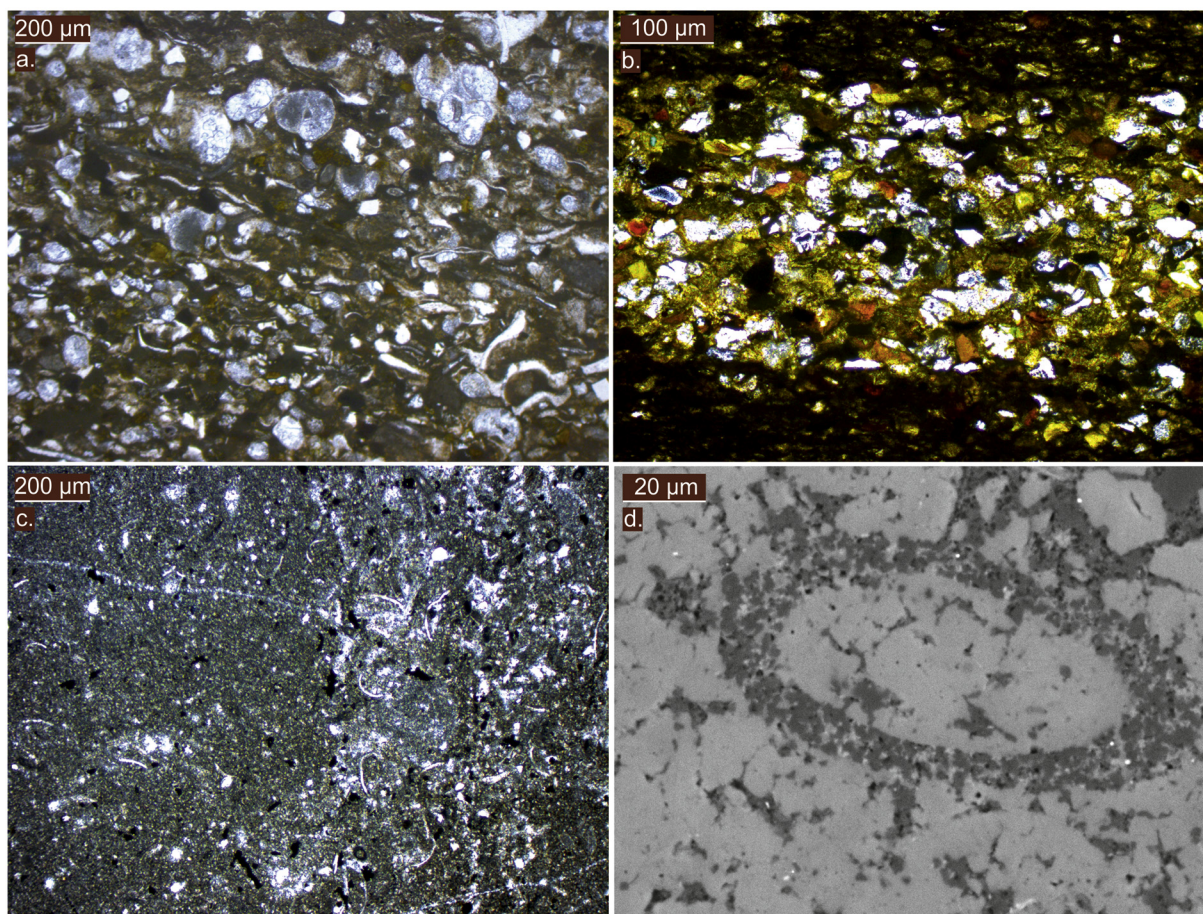

Fig. 2. Sedimentary log of the Permo-Triassic boundary beds at Jiucaichong in southwest Guizhou and at Chinahe, north-east Yunnan.

Fig. 3. Photomicrographs and SEM image of Permo-Triassic boundary strata from SW China. (a). Bed 4 at Zhonghe section showing abundant microgastropods and grains of chamosite and kaolinite (Zhg-5). (b) Photomicrograph of chamositic sandstone from 4.75 *m* height in the Chinahe section (see Fig. 2). Some chamosite grains have weathered to an orange colour but others retain their bright green colour. The opaque grains are intraclasts of kaolinite, reworked (like the chamosite grains) from interbedded mudstones and coals. (c) Micritic mudstone (Bed 5) found in the cavities between thrombolites at Zhonghe, showing abundant opaque pyrite crystals and ostracod valves. (d) SEM image of *Earlandia* from Bed 30 at Zhongzhai showing an agglutinated test composed of micron-sized grains of quartz embedded in a matrix of carbonate. (For interpretation of the references to colour in this figure legend, the reader is referred to the web version of this article.)

minor mudstone and coal beds (Fig. 2). The sandstone beds are tabular, sharp based, massive and range from fine to coarse grained. Petrographic examination reveals both the sandstone and siltstone to be mostly composed of angular grains of chamosite with kaolinite intraclasts, charcoal fragments and minor quartz, feldspar and rutile grains (Fig. 3b). Similar sandstone and siltstone beds compromise the basal two metres of the Kayitou Formation, with cm-sized charcoal grains being especially common in the former. These are overlain by a 1.5 m-thick grey-green mudstone (with tabular carbonate concretions), that yields a low diversity marine fauna (*Neoschizodus*, *Promyalina* and *Lingula*) and *E. gutta*. The succeeding strata gradually coarsen-upwards as thin sand laminae appear, initially only a few millimetres thick that eventually become 1–2 cm thick. *Lingula* occurrences persist up to this level. Pyrite framboids occur in the mudstones (Fig. 2), albeit rarely, and exhibit a generally large size (diameters of 7–30 μm) typical of framboids that form in weakly dysoxic conditions today (cf. Bond and Wignall, 2010). Pyrite is otherwise absent from the Chinahe section.

The lower coal bed in our logged section rests on a mature palaeosol (pale grey mudstone with abundant rootlets) whilst the upper coal bed is somewhat fissile (rather than blocky) and rests on carbonaceous shale. It is likely that the upper coal records re-sedimentation of plant material whilst the lower coal bed is an in situ peat accumulation. A diverse Permian plant flora is encountered up to 4 *m* above the base of our measured section, slightly below where the marine fauna appears.

Overall the Chinahe depositional environment consisted of low

energy, swamp environments subject to erosive flood events that exhumed authigenic chamosite and kaolinite intraclasts. The increased abundance of charcoal in the latest Permian strata also testifies to more frequent and/or intense wildfires (Yan et al., 2019; Chu et al., 2020). It was during these prevailing conditions that the floral mass extinction occurred. The subsequent grain-size decrease and appearance of a Triassic marine fauna (Song et al., 2019) indicates coastline retreat and a temporary transition to a low energy, inner shelf setting before a return to freshwater swamp conditions.

The bulk $\delta^{13}C_{org}$ values from the Xuanwei Formation provide information on the timing of the extinction at Chinahe (Chu et al., 2020). Values decline slightly from −24‰ to −25‰ in the topmost 25 *m* of the Formation and then show a rapid negative trend in the basal 4 *m* of the Kayitou Formation reaching a lowpoint of ∼ − 30‰. The floral mass extinction occurs during this rapid ∼6‰ negative shift whilst the marine bivalves, characteristic of the immediate post mass extinction fauna, appears just below the $\delta^{13}C_{org}$ minimum. The floral extinction therefore started before the marine extinction with both events occurring within the latest Permian (Chu et al., 2020). A second, less distinct $\delta^{13}C_{org}$ lowpoint occurs 10 *m* above the base of the Kayitou Formation (Chu et al., 2020) above the level studied here.

4.3. Borehole N3

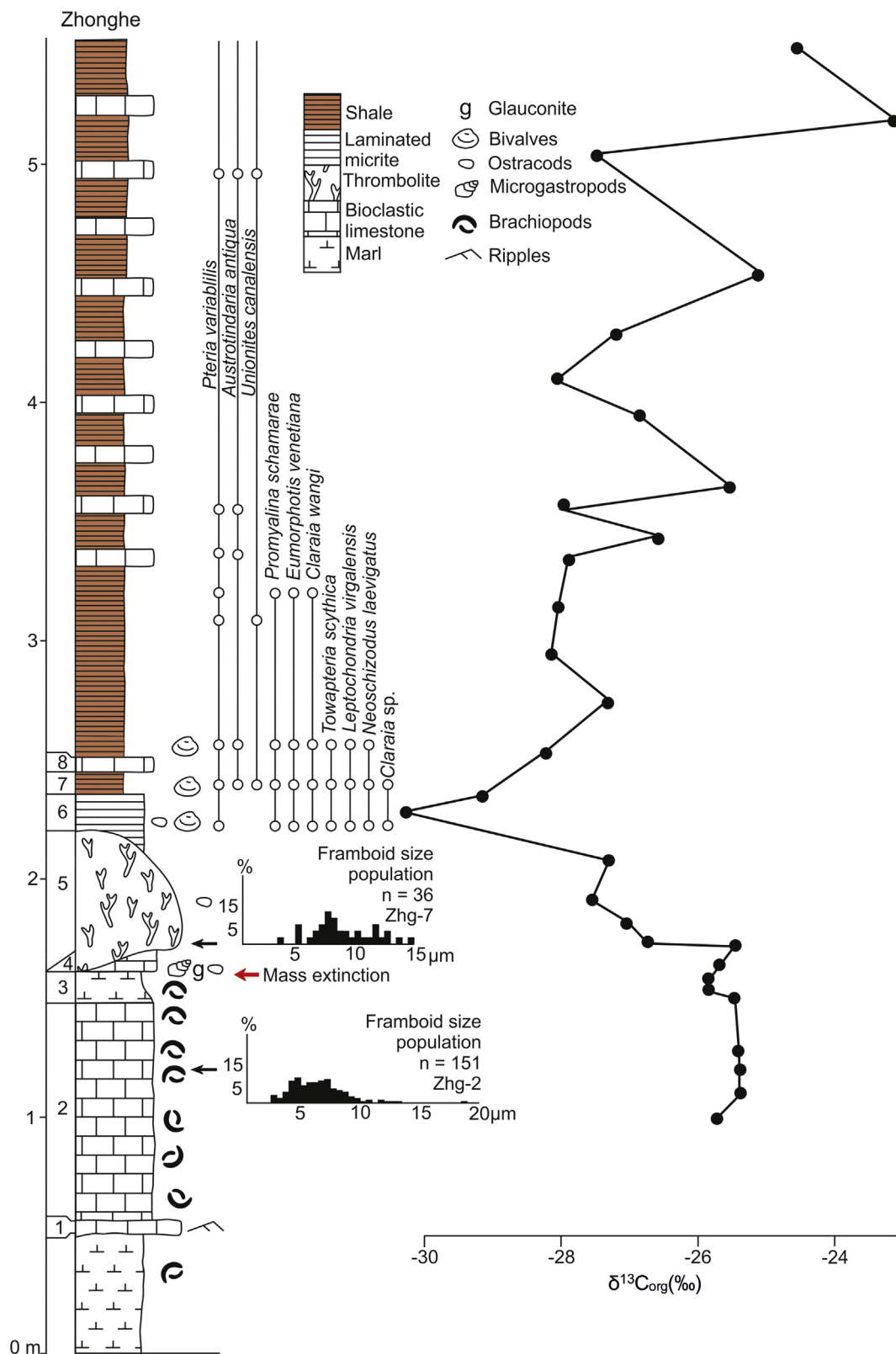The Xuanwei Formation in the N3 core consists of numerous coal,

Fig. 4. Sedimentary log of the Zhonghe section showing local development of thrombolitic mounds, bivalve range chart, size distributions of framboid populations (where present) and $\delta^{13}C_{org}$ trends.

shale and green sandstone beds. The latter range from a few centimetres up to 10 m in thickness and are most abundant in the basal 15% and topmost 40% of the Formation. The sandstones range from fine to medium grained and are frequently calcareous with both grains of

carbonate and carbonate cement present, especially in the lower two-thirds of the Formation. Otherwise the beds consist of angular grains of varying proportions of feldspar, chert, chamosite and kaolinite. Other than the feldspar grains, which are likely eroded from the Emeishan

basalts in the Kangdian hinterland, the other minerals all occur as common diagenetic phases in Xuanwei coals (Dai and Chou, 2007; Dai et al., 2014). Thus, the sandstone beds likely record frequent and substantial erosion of the peat swamps throughout the depositional history of the Xuanwei Formation, resulting in the transport and concentration of these diagenetic minerals.

4.4. Zhonghe section

The Zhonghe section contains a marine fauna throughout and records more offshore conditions than the sections described above (Fig. 4). The uppermost Longtan Formation is dominated by mudstone beds but these are sharply overlain by a thin, ripple cross laminated grainstone (Bed 1) and a wackestone (Bed 2) that becomes marly in its uppermost 10 cm (Bed 3). Beds 2 and 3 contain abundant ostracods and brachiopods (often silicified) that include *Fusichonetes pygmaea*, *Neochonetes* sp., and *Spinomarginifera* sp.. The marl of Bed 3 is overlain by an impersistent limestone (Bed 4) with abundant spar-filled microgastropods, ostracods and small foraminifers (Fig. 3b) and abundant sand-grade grains of kaolinite that are either pellets or small mud chips. SEM analysis of this muddy limestone reveals that, in additional to kaolinite grains, there are also silt-grade grains of quartz and chamosite-kaolinite intergrowths but no pyrite.

Bed 4 and the strata overlying it show considerable lateral variation. Broad thrombolite domes (Bed 5), up to 2 m wide and 45 cm thick, are developed and these locally rest directly on Bed 3 (Fig. 5). A bed of pale, pyritic wackestone with foraminifers (*Earlandia*) and small ostracods occurs in between the thrombolite domes and can be up to 15 cm thick. The pyrite content of the wackestone includes common crystals visible in thin section (Fig. 3c) and large framboids (seen in SEM) typical of those formed in upper dysoxic environments (Fig. 4). The thrombolites are draped by a thin-bedded, pyritic, wackestone (Bed 6) with common bivalves, microconchids, *Earlandia*, ostracods and *Hindeodus praeparvus* (Fig. 5). The pyrite content in Bed 6 is dominated by crystals and SEM analysis reveals only occasional framboids. Bivalves become moderately diverse at this level (Fig. 4) and belong to the *Promyalina-Neoschizodus* community that is widespread in lowermost Triassic strata in the coastal facies of SW China (Song et al., 2019). The bivalve assemblage ranges into the overlying grey-green mudstone/thin micrite interbeds but becomes progressively less diverse, although ostracods continue to be abundant at these higher levels.

The position of the PTME at Zhonghe can be placed precisely at the boundary between beds 3 and 4 where abundant brachiopods disappear to be replaced by microgastropods (Fig. 3c), that typically bloom in the aftermath of the Permian – Triassic mass extinction in many locations throughout the world (e.g. Fraiser et al., 2005). Comparison with the bulk $\delta^{13}C_{org}$ record generated for this section shows the extinction coincides with the start of a negative excursion, which reaches a lowpoint just above the thrombolite bed. Detailed studies of bulk $\delta^{13}C$ values, especially at the Meishan PTB stratotype often reveal two distinct lowpoints (Xie et al., 2007; Joachimski et al., 2012; Yin et al., 2014): a first spanning the *H. changxingensis* Zone, above the first phase of extinction and a brief lowpoint in the *I. isarcica* Zone immediately above a second phase. The $\delta^{13}C_{org}$ record at Zhonghe shows the onset of a single negative excursion starting at the bed 4/5 boundary and reaching a lowpoint in Bed 6 (Fig. 4). The start of the excursion "jumps" abruptly and the sharp nature of the bed contact at this level, together with the local cut-out of Bed 4 (Fig. 5) suggests there is likely to be a hiatus at this point. The first negative excursion may therefore be missing in this gap, a common occurrence in the shallow-marine sections of South China (Yin et al., 2014). Thus, the thrombolite bed at Zhonghe may be of earliest Triassic age (the presence of *H. praeparvus* in the overlying bed only indicates a PTB age because this conodont ranges across the boundary). Elsewhere in South China, microbialite beds began forming
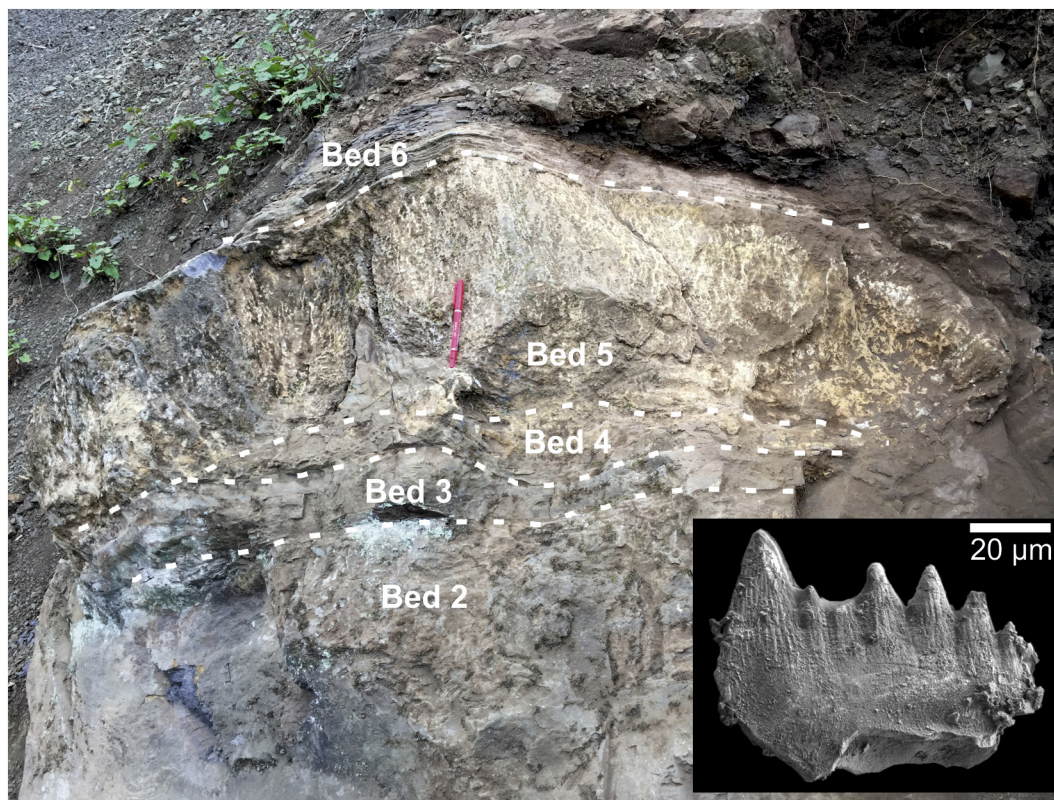

Fig. 5. Permo-Triassic boundary beds at Zhonghe. The mass extinction occurs between beds 3 and 4. Note that Bed 4 is cut out at the base of the thrombolite at the left-hand side of the view. To the left of the pen a wedge-shaped cavity beneath two thrombolite "heads" has been infilled with micritic mudstone seen in Fig. 3c. Inset shows a specimen of *Hindeodus praeparvus* from Bed 6.

just above the onset of the main extinction phase in the latest Permian, but became much more widespread in the basal Triassic *Hindeodus parvus* Zone (Kershaw et al., 2012; Wang et al., 2016; Tang et al., 2017), and the Zhonghe example may be of this age.

4.5. Langdai sections

At both Langdai sections the uppermost metre of the Longtan Formation consists of brown-weathering mudstone with abundant plant remains and small brachiopods (especially chonetids). This is overlain by a 2 cm-thick pale ash bed and a 1 cm-thick sandy mudstone composed of chamosite, chert and dolomite grains in a kaolinitic mud matrix. These beds mark the base of the Feixuanguan Formation and, at Langdai-2 it passes upwards into several metres of yellow-green mudstone of the Feixuanguan Formation. The associated fauna consists of *Claraia* and microgastropods – a typical post mass extinction assemblage that indicates the Permo-Triassic boundary occurs at the formation boundary. At Langdai-1, at the base of the Feixianguan Formation there is a 38 cm-thick, impersistent horizon of microbialite limestone lenses, which are overlain by and pass laterally into yellow-green mudstone. In thin section the limestone displays a thrombolitic texture and both *Earlandia* and pyrite crystals are seen to be common in the microbialite.

4.6. Zhongzhai section

At Zhongzhai the PTB boundary sediments consist of high energy, open marine limestone facies that sharply overlie mudstone beds of the Longtan Formation (Metcalfe and Nicoll, 2007). Initially, a packstone (Bed 28a) is developed, with a diverse Permian fauna of brachiopods, foraminifers (including fusulinids), echinoderms and bryozoans. This is overlain by Bed 28b, a grainstone with a similar albeit much more abraded fossil assemblage and rounded grains of glauconite and phosphate. Following a white ash (Bed 29), the succeeding Bed 30 consists of thin-bedded grainstone, in which centimetre-thick, graded beds contain a typical post mass extinction fauna: ostracods, bivalves, *Earlandia* and microconchids. SEM analysis revealed no pyrite in these beds although small grains of phosphate are common in Bed 30. The *Earlandia* tests are seen to be agglutinated and composed of micron-sized quartz grains (Fig. 3d).

5. Discussion

5.1. Sedimentary environments and climate

The lateral transition from terrestrial to nearshore shallow marine settings in the Permo-Triassic WGEY sections occurs in an overall low energy environment dominated by mudstone facies. In the terrestrial sections the mudstones do not show evidence for emergence, except beneath the thin coal seams, suggesting deposition occurred in floodplain lakes. Sheet sandstones are also important in the more proximal settings of the Xuanwei and Kayitou formations, where lenticular, channel sandstone bodies also occur (Bercovici et al., 2015). The component sand grains of these green sandstones almost entirely consist of reworked diagenetic material (chamosite and kaolinite) that has been sourced from the associated coal and mudstone beds. Frequent and substantial erosion of lacustrine and peat deposits during flood events was therefore the source of much of the arenaceous material. Minor contributions of detrital sediment (feldspar and rutile grains) are likely from the Emeishan basalt hinterland to the west. The abundance of charcoal fragments in both the mudstone and sandstone bed also suggests frequent wildfires and therefore intermittent aridity (Chu et al., 2020). Combined together, it would appear that the climate during the Permo-Triassic transition was one of extremes: intense rainfall and flooding interspersed with drier periods marked by wildfires. Interestingly, a similar climatic situation has been proposed for the terrestrial PTB sections in South Africa (MacLeod et al., 2017; Smith and Botha-Brink, 2014), even though this far-distant region was in high southern latitudes rather than the tropical location of South China.

The fine-grained clastic nature of the PTB sediments in WGEY has been attributed to low-energy deposition in the lee of a barrier island system resulting in the interpretation of the Longtan and Kayitou formations as "lagoonal" facies (Bercovici et al., 2015). However, a stenohaline fauna (e.g. brachiopods and bryozoans) occur prior to the extinction indicating normal salinities and open marine connections. Perhaps in tacit acknowledgment of this, the facies model of Bercovici et al. (2015) show only small, widely separated offshore barrier islands, which raises the question of why a low energy, mud-dominated coastal facies belt developed in an open marine setting? Thin beds (< 1 cm thick) of kaolinite and chamosite grains occur at the PTB in the shallow-marine Langdai location but generally only clay-grade detrital material reached shelf settings. It seems depositional gradients may have been very low thus limiting transport by tractional processes. Only the carbonate boundary sediments at Zhongzhai show evidence for persistent agitation (abraded grains, lack of fine-grained matrix) and this relatively offshore location, beyond the reach of clastic input (at least during the PTB interval), may have lain close to a shelf margin outboard of a tranquil, coastal mud-belt.

Similar terrestrial and coastal PTB transitions have been interpreted to record major environmental and climatic changes during the mass extinction interval. A change from meandering to braided channels seen in South Africa and elsewhere has been linked with plant mass extinction and consequent decrease in bank stability (Ward et al., 2000), although a switch to more arid conditions has also been mooted as a possible cause of the change in fluvial style (Zhu et al., 2019). Forest die-off in Australia has also been suggested to have raised regional water tables (Vajda et al., 2020). There is no evidence for any of these changes in the PTB interval in WGEY, although the terrestrial sections all show an increase in mudstone at the expense of sandstone. This change is probably best linked with a base-level rise of likely eustatic origin.

5.2. Sea-level change

The relationship between sea-level change and mass extinction during the PTB interval has been the subject of much debate (Hallam and Wignall, 1999). In the open marine sections of South China there is evidence for a minor (type 2) sequence boundary in the late *Clarkina yini* Zone that resulted in the succeeding *C. meishanensis* Zone being frequently absent from shallow, carbonate platform sections (Yin et al., 2014). Subsequent transgression saw deposition re-established in most shallow marine areas during the *Hindeodus changxingensis* Zone, and conditions continued to deepen across the PTB and into the Early Triassic (Yin et al., 2014). In the more complete, deeper-water settings the first/main phase of mass extinction occurred in the earliest part of this transgression. Thus, at Meishan the sequence boundary has been placed between beds 24d and 24e and the extinction occurs at the top of Bed 24e (Yin et al., 2014). In shallower sections, the extinction occurs at the hiatal contact between the underlying highstand systems tract and the overlying transgressive systems tract. So how does the sea level/extincton record in the paralic sections of WGEY compare?

In the terrestrial sections of WGEY (e.g. Chinahe and Jiucaichong) the youngest Permian hiatus is recorded at the top of the topmost palaeosol of the Xuanwei Formation (Fig. 6). The overlying succession fines upwards and deepens to the point whereby a marine fauna appears at Chinahe, although not in the more proximal Jiucaichong section. Like the carbonate platform successions of South China, this record appears to consist of a highstand systems tract separated by a sequence boundary from a transgressive systems tract (Fig. 6) It is unsurprising that no lowstand or shelf margin system tract occurs because such strata are only likely to be develop down-dip in more offshore settings. More distally, in the shallow marine sections of WGEY
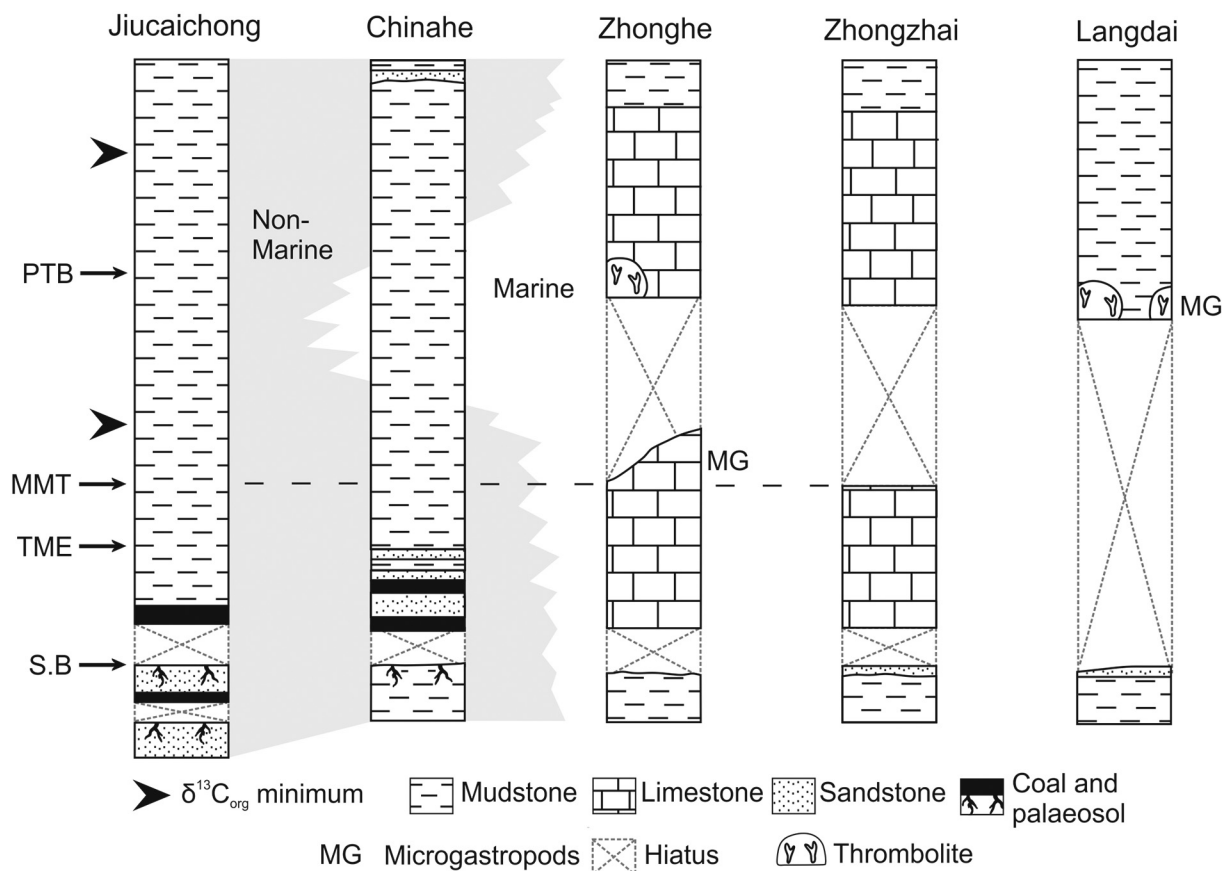
Fig. 6. Schematic, chronostratigraphic correlation panel of the study sections in southwest China. Timelines are provided by two lowpoints in the $\delta^{13}C_{org}$ record that straddle the PTB. Relative timing of marine (MME) and terrestrial (TME) mass extinctions is from Chu et al. (2020). S.B. sequence boundary, PTB Permo-Triassic boundary.

the sequence boundary occurs at the sharp contact/abrupt shallowing seen between the mudstone and topmost limestones of the Longtan Formation (base of Bed 1 at Zhonghe; base of Bed 28a at Zhongzhai). The mm-thick bed of green sandstone at this contact at Zhongzhai records terrigenous influx and could be the feather edge of a thicker sandstone package (a shelf margin wedge?) developed downdip. Within the PTB carbonates it is likely there is another hiatus (Fig. 6). The "jump" in the $\delta^{13}C_{org}$ values at the Bed 3/4 boundary at Zhonghe and at the top of Bed 29 at Zhongzhai and the absence of the first $\delta^{13}C_{org}$ minimum at these locations suggests a hiatus at these contacts (Fig. 6). This could record another sequence boundary, but sediment starvation due to a failure of carbonate production could be responsible. In the most distal Langdai sections the sharp contact between the Longtan and Yelang formations is interpreted to record a prolonged hiatus (Fig. 6) again reflecting a failure of sediment supply although this interpretation requires corroborating $\delta^{13}C_{org}$ evidence.

5.3. Marine extinction causes

Ocean acidification has been proposed as a primary cause of the marine losses at the end of the Permian (Payne et al., 2007; Lehrmann et al., 2015). The principal evidence is a truncation surface, that is well seen in carbonate platform settings in Guizhou Province, 100–200 km east of our study area, that have been attributed to submarine dissolution. This surface has been alternatively interpreted as a karstic surface caused by regression (Wignall et al., 2009; Collin et al., 2009; Yin et al., 2014; Baresel et al., 2017). A latest Permian regression is also seen in the clastic, paralic successions of WGEY, and in many locations around the world (Hallam and Wignall, 1999), and also on the shallow shelf where carbonate abruptly succeeds mudstone (Fig. 6). However, a

truncation surface is also developed at a slightly higher stratigraphic level within the carbonate beds (Fig. 6). This occurs around the mass extinction level raising the possibility that submarine dissolution occurred at this time. However, in detail, the truncation surface only occurs at the mass extinction level at Zhongzhai whilst it occurs above it at Zhonghe.

If the WGEY record offers equivocal evidence for an acidification-driven crisis then what about other potential extinction drivers in the shallow seas? Massive die-off of terrestrial vegetation is likely to have been followed by rapid erosion of the denuded soils. Support for such a scenario comes from the increased supply of soil-derived biomarkers in western Tethyan PTB sections (Sephton et al., 2005) and "poorly sorted breccias" (interpreted as soil erosion products) reported from WGEY successions (Zhang et al., 2016). Such observations have helped develop the idea that a major increase of sedimentation in marine habitats, was substantially responsible for the marine mass extinction – a death-by-siltation kill mechanism, that was abetted by an increased supply of nutrients leading to eutrophication (Algeo and Twitchett, 2010; Algeo et al., 2011; Kaiho et al., 2016; Vajda et al., 2020). Potential support for high clastic input in WGEY comes from the presence of green sandstones, composed of authigenic material (chamosite and kaolinite) supplied by erosion of coals and lacustrine mudstones. These indicate substantial erosion was occurring during flood events in terrestrial environs. However, the green sandstone beds are present throughout the Changhsingian Stage, as recorded in the N3 core, and they persist into the Early Triassic indicating that the erosive episodes were a prevailing feature of deposition over several million years: there is no evidence for a surge in terrestrial influx at the PTB. It is also important to note that reports of poorly-sorted breccia beds (Zhang et al., 2016), come from the Dongchuan Formation. This stratigraphic

unit overlies the Kayitou Formation, and is considerably younger than the extinction interval. Contrary to claims of increased sediment influx during the PTME, the WGEY boundary sediments record a temporary shutdown of clastic sedimentation in shallow shelf settings with mudstones being replaced by limestones, whilst the terrestrial sections record a decline in the sandstone:mudstone ratio. These observations likely reflect sediment entrapment in aggrading coastal plains during the transgression (a typical phenomenon during all intervals of transgression).

With neither acidification nor siltation looking like strong contenders for marine kill mechanisms, what about the role of anoxia in our nearshore study sections? The main phase of marine mass extinction is best seen in the Zhonghe section, at the boundary between beds 3 and 4, and in the Zhongzhai section between beds 28b and 30 (the intervening Bed 29 is a volcanic ash). At Zhonghe the youngest Permian taxa occur in a bed with large framboids that indicate upper dysoxic conditions (Fig. 4). Following the mass extinction, the microgastropod packstone (Bed 4) lacks pyrite, although glauconite grains are common. Upper dysoxic framboid populations return in the micrite bed that occurs in between the thrombolite domes at this location. Pyrite is lacking from the PTB packstones and grainstone beds at Zhongzhai however glauconite and phosphate grains are both present. The Langdai boundary sediments also lack framboids although pyrite crystals are present in the basal Triassic strata. Clearly, none of these nearshore boundary sections records intense anoxia associated with the Permo-Triassic mass extinction. Nonetheless, glauconite and phosphate are both minerals that indicate deposition either at the redox boundary or under an oscillating redox regime (Odin and Létolle, 1980; O'Brien et al., 1990; Algeo and Ingall, 2007), whilst the framboids suggest upper dysoxic conditions. For the majority of marine invertebrates such conditions are highly stressful and reduce available habitat area suggesting oxygen-poor conditions played a role in the shallow-water crisis.

Anoxia during the PTB has been linked to warming (Sun et al., 2012) and this factor could also have been a stress in shallow waters. The general association of small body size with high temperatures is thought to explain the diminutive size of gastropods in the immediate aftermath of end-Permian extinction (e.g. Pietsch et al., 2014). Microgastropods were prolifically abundant immediately after the extinction in WGEY (Fig. 6) in accord with the role of elevated temperatures in the crisis. Interestingly this bloom of disaster taxa was short-lived, the succeeding beds are dominated by bivalves: low diversity *Claraia* populations in the more offshore Langdai sections and a more diverse *Promyalina-Neoschizodus* assemblage in coastal settings (Song et al., 2019)

There has been considerable debate about oxygenation levels during microbialite formation. Some have suggested thrombolites grew in dysoxic conditions (Pruss et al., 2006; Wang et al., 2016) in accord with our observations reported here (e.g. the dysoxic framboid populations in the thrombolite level at Zhonghe). However, others have reported oxic conditions during microbialite formation (Kershaw et al., 2012; Loope et al., 2013; Lehrmann et al., 2015; Tang et al., 2017). The presence of moderately diverse, associated ostracod communities has led to suggestions that microbialite environments provided oxic refuges during the crisis (Forel, 2013). If so it was only a temporary one, a second pulse of extinction in the earliest Triassic eliminated many of the microbialite-associated ostracods at the end of the *H. parvus* Zone (Song et al., 2013). Given the diversity of evidence from different locations it seems likely that the microbialites grew in conditions spanning a spectrum from oxia to dysoxia. Whether these redox conditions are pertinent to the debate about the cause of the PTME is another matter, because the main extinction occurred prior to the formation of microbialites (Jiang et al., 2014).

6. Conclusion

The paralic PTB sections of WGEY record a severe mass extinction indicating that the nearest-shore settings in south-western China did not provide a refuge from the environmental vicissitudes of the time. They also provide evidence to show that many of the favoured mass extinction mechanisms were unlikely to have operated, at least in this region. Thus, the siltation model (extinction caused by rapid burial due to a drastic increase of terrestrial sediment influx) is not supported because the boundary interval saw a shut-down of clastic influx with carbonates (including microbialites) replacing mudstones. This may reflect the trapping of terrigenous material in aggrading coastal plains during a phase of base-level rise. A minor regression occurred shortly before the extinction and is manifest as an abrupt shallowing in shallow marine sections and a palaeosol in terrestrial locations. A truncation/hiatal surface is also seen within the PTB carbonates which recalls similar surfaces seen in more easterly locations (e.g. carbonate platforms in southern Guizhou) which have been attributed to the effects of ocean acidification. However, the hiatal surface slightly postdates the mass extinction in one section and it is possible the surface reflects a failure of carbonate production in the immediate aftermath of the extinction rather than a loss of dissolution.

Despite the nearshore, shallow-water setting of the WGEY locations, oxygen-poor seafloor conditions were prevalent during the PTB interval, as manifest by the presence of dysoxic framboid populations, glauconite and phosphate grains. Unsurprisingly, the oxygen restriction was a good deal less intense than seen in more offshore, deeper settings but would nonetheless have imposed stresses on marine life. A brief bloom of microgastropods immediately after the mass extinction, also seen in many other sections around the world, could indicate dwarfing due to high temperatures during the crisis, although this stressor is better indicated by more direct proxies such as oxygen isotopes.

Declaration of Competing Interest

We declare that there are no conflicts of interest associated with this manuscript.

References

Algeo, T.J., Ingall, E., 2007. Sedimentary C$_{org}$:P ratios, paleoocean ventilation, and Phanerozoic atmospheric pO$_2$. Palaeogeogr. Palaeoclimatol. Palaeoecol. 256, 130–155. https://doi.org/10.1016/j.palaeo.2007.02.029.

Algeo, T.J., Twitchett, R.J., 2010. Anomalous early Triassic sedimentary fluxes due to elevated weathering rates and their biological consequences. Geology 38, 1023–1026. https://doi.org/10.1130/G31203.1.

Algeo, T.J., Chen, Z.Q., Fraiser, M.L., Twitchett, R.J., 2011. Terrestrial-marine teleconnections in the collapse and rebuilding of early Triassic marine ecosystems. Palaeogeogr. Palaeoclimatol. Palaeoecol. 308, 1–11. https://doi.org/10.1016/j.palaeo.2011.01.011.

Baresel, B., Bucher, H., Bagherpour, B., Brosse, M., Guodun, K., Shaltegger, U., 2017. Timing of regression and microbial bloom linked with the Permian-Triassic boundary mass extinction: implications for driving mechanisms. Sci. Rep. 7, 43630. https://doi.org/10.1038/srep43630.

Benton, M.J., Newell, A.J., 2014. Impacts of global warming on Permo-Triassic terrestrial ecosystems. Gondwana Res. 25, 1308–1337. https://doi.org/10.1016/j.gr.2012.12.010.

Benton, M.J., Twitchett, R.J., 2003. How to kill (almost) all life: the end-Permian extinction event. Trends Ecol. Evol. 18, 358–365. https://doi.org/10.1016/S0169-5347(03)00093-4.

Bercovici, A., Cui, Y., Forel, M.-B., Yu, J.X., Vajda, V., 2015. Terrestrial paleoenvironmental characterization across the Permian-Triassic boundary in South China. J. Asian Earth Sci. 98, 225–246. https://doi.org/10.1016/j.jseaes.2014.11.016.

Bond, D.P.G., Wignall, P.B., 2010. Pyrite framboid study of marine Permo-Triassic boundary sections: a complex anoxic event and its relationship to contemporaneous mass extinction. Bull. Geol. Soc. Am. 122, 1265–1279. https://doi.org/10.1130/B30042.1.

Briggs, D.E.G., Gall, J.C., 1990. The continuum in soft-bodied biotas from transitional environments: a quantitative comparison of Triassic and Carboniferous Konservat-Lagerstätten. Paleobiol. 16, 204–218. https://doi.org/10.1017/S009483730000988.

Buatois, L.A., Gingras, M.K., Maceachern, J., Mángano, M.G., Zonneveld, J.-P., 2005. Colonization of brackish water ecosystems through time: evidence from the trace-fossil record. Palaios 20, 321–347. https://doi.org/10.2110/palo.2004.p04-32.

Chu, D.L., Yu, J.X., Tong, J.N., Benton, M.J., Song, H.J., Huang, Y.F., Song, T., Tian, L., 2016. Biostratigraphic correlation and mass extinction during the Permian-Triassic transition in terrestrial-marine siliciclastic settings of South China. Glob. Planet. Chang. 146, 67–88. https://doi.org/10.1016/j.gloplacha.2016.09.009.

Chu, D.L., Grasby, S.E., Song, H.J., Dal Corso, J., Wang, Y., Mather, T.A., Wu, Y.Y., Song, H.Y., Shu, W.C., Tong, J.N., Wignall, P.B., 2020. Ecological disturbance in tropical peatlands prior to marine Permo-Triassic mass extinction. Geology 48, 288–292. https://doi.org/10.1130/G46631.1.

Collin, P.Y., Kershaw, S., Crasquin-Soleau, S., Feng, Q., 2009. Facies changes and diagenetic processes across the Permian-Triassic boundary event horizon, Great Bank of Guizhou, South China: a controversy of erosion and dissolution. Sedimentology 56, 677–693. https://doi.org/10.1111/j.1365-3091.2008.00992.x.

Dai, S.F., Chou, C.L., 2007. Occurrence and origin of minerals in a chamosite-bearing coal of late Permian age, Zhaotang, Yunnan. China. Amer. Mineral. 92, 1253–1261. https://doi.org/10.2138/am.2007.2496.

Dai, S.F., Li, T., Seredin, V.V., Ward, C.R., Hower, J.C., Zhou, Y.P., Zhang, M.Q., Song, X.L., Song, W.J., Zhao, C.L., 2014. Origin of minerals and elements in the late Permian coals, tonsteins, and host rocks of Xinde Mine, Xuanwei, eastern Yunnan. Int. J. Coal Geol. 121, 53–78. https://doi.org/10.1016/j.coal.2013.11.001.

Forel, M.B., 2013. The Permian-Triassic mass extinction: Ostracods (Crustacea) and microbialites. Compt. Rendus Geosci. 345, 203–211. https://doi.org/10.1016/j.crte.2013.03.003.

Fraiser, M.L., Twitchett, R.J., Bottjer, D.J., 2005. Unique microgastropod biofacies in the early Triassic: Indicator of long-term biotic stress and the pattern of biotic recovery after the end-Permian mass extinction. Compt. Rend. Palevol. 4, 543–552. https://doi.org/10.1016/j.crpv.2005.04.006.

Hallam, A., Wignall, P.B., 1999. Mass extinctions and sea-level changes. Earth-Sci. Rev. 48, 217–250. https://doi.org/10.1016/S0012-8252(99)00055-0.

He, X.Y., Wang, S.J., Wang, J., Hilton, J., 2019. The anatomically preserved tri-pinnate frond *Rothwellopteris marginata* gen. Et. Comb. nov. from the latest Permian of South China: timing the stem to crown group transition in Marattiales. Int. J. Plant Sci. 180, 869–881. https://doi.org/10.1086/704946.

Huang, Y.G., Chen, Z.Q., Wignall, P.B., Zhao, L.S., 2017. Latest Permian to Middle Triassic redox condition variations in ramp settings, South China: Pyrite framboid evidence. Bull. Geol. Soc. Am. 129, 229–243. https://doi.org/10.1130/B31458.1.

Jiang, H.S., Lai, X.L., Sun, Y.D., Wignall, P.B., Liu, J.B., Yan, C.B., 2014. Permian-Triassic conodonts from Dajiang (Guizhou, South China) and their implication for the age of microbialite deposition in the aftermath of the end-Permian mass extinction. J. Earth Sci. 25, 413–430. https://doi.org/10.1007/s12583-014-0444-4.

Joachimski, M.M., Lai, X.L., Shen, S.Z., J, H.S., Luo, G.M., Chen, B., Chen, J., Sun, Y.D., 2012. Climate warming in the latest Permian and the Permian-Triassic mass extinction. Geology 40, 195–198. https://doi.org/10.1130/G32707.1.

Kaiho, K., Saito, R., Ito, K., Miyaji, T., Biswas, R., Tian, L., Sano, H., Shi, Z.Q., Takahashi, S., Tong, J.N., Liang, L., Oba, M., Nara, F.W., Tsuchiya, N., Chen, Z.Q., 2016. Effects of soil erosion and anoxic-euxinic ocean in the Permian-Triassic marine crisis. Heliyon 2, e00137. https://doi.org/10.1016/j.heliyon.2016.e00137.

Kershaw, S., Crasquin, S., Li, Y., Collin, P.-Y., Forel, M.-B., Mu, X., Baud, A., Wang, Y., Xie, S., Maurer, F., Guo, L., 2012. Microbialites and global environmental change across the Permian-Triassic boundary: a synthesis. Geobiol. 10, 25–47. https://doi.org/10.1111/j.1472-4669.2011.00302.x.

Lehrmann, D.J., Bentz, J.M., Wood, T., Goers, A., Dhillon, R., Akin, S., Li, X.W., Payne, J.L., Kelley, B.M., Meyer, K.M., Schaal, E.K., Suarez, M.B., Yu, M.Y., Qin, Y.J., Minzoni, M., Henderson, C.M., 2015. Environmental controls on the genesis of marine microbialites and dissolution surface associated with the end-Permian mass extinction: new sections and observations from the Nanpanjiang Basin, South China. Palaios 30, 529–552. https://doi.org/10.2110/palo.2014.088.

Loope, G.R., Kump, L.R., Arthur, M.A., 2013. Shallow water redox conditions from the Permian-Triassic boundary microbialite: the rare earth element and iodine geochemistry of carbonates from Turkey and South China. Chem. Geol. 351, 195–208. https://doi.org/10.1016/j.chemgeo.2013.05.014.

MacLeod, K.G., Quinton, P.C., Bassett, D.J., 2017. Warming and increased aridity during earliest Triassic in the Karoo Basin, South Africa. Geology 45, 483–486. https://doi.org/10.1130/G38957.1.

Metcalfe, I., Nicoll, R.S., 2007. Conodont biostratigraphic control on transitional marine to non-marine Permian-Triassic boundary sequences in Yunnan-Guizhou, China. Palaeogeogr. Palaeoclimatol. Palaeoecol. 252, 56–65. https://doi.org/10.1016/j.palaeo.2006.11.034.

Nicoll, R.S., Metcalfe, I., 2005. Chronostratigraphic and biostratigraphic control on the Permian-Triassic boundary in the Zhongzhai section, Guizhou Province. Albertiana 33, 64.

O'Brien, G.W., Milnes, A.R., Veeh, H.H., Heggie, D.T., Riggs, S.R., Cullen, D.J., Marshall, J.F., Cook, P.J., 1990. Sedimentation dynamics and redox iron cycling: Controlling factors for the apatite glauconite association on the East Australian continental margin. In: Notholt, A.J.G., Jarvis, I. (Eds.), Phosphorite Research and Development: Geol. Soc. [London] Spec. Pub. 52. pp. 61–86. https://doi.org/10.1144/GSL.SP.1990.052.01.06.

Odin, G.S., Létolle, R., 1980. Glauconitization and phosphatization environments: A tentative comparison. In: Bentor, Y.K. (Ed.), Marine Phosphorites: Soc. Econ. Paleo. Mineral. Spec. Pub 29. pp. 227–237.

Payne, J.L., Lehrmann, D.J., Follet, D., Seibel, M., Kump, L.R., Riccardi, A., Altiner, D., Sano, H., Wei, J., 2007. Erosional truncation of uppermost Permian shallow-marine carbonates and implications for Permian-Triassic boundary events. Bull. Geol. Soc. Am. 11, 771–784. https://doi.org/10.1130/B26091.1.

Peng, Y.Q., Zhang, S.X., Yu, T.X., Yang, F.Q., Gao, Y.Q., Shi, G.R., 2005. High-resolution terrestrial Permian-Triassic eventstratigraphic boundary in western Guizhou and eastern Yunnan, southwestern China. Palaeogeogr. Palaeoclimatol. Palaeoecol. 215, 285–295. https://doi.org/10.1016/j.palaeo.2004.09.009.

Pietsch, C., Mata, S.A., Bottjer, D.J., 2014. High temperature and low oxygen perturbations drive contrasting benthic recovery dynamics following end-Permian mass extinction. Palaeogeogr. Palaeoclimatol. Palaeoecol. 399, 98–113. https://doi.org/10.1016/j.palaeo.2014.02.011.

Pruss, S.B., Bottjer, D.J., Corsetti, F.A., Baud, A., 2006. A global marine sedimentary response to the end-Permian mass extinction: examples from southern Turkey and the western United States. Earth-Sci. Rev. 78, 193–206. https://doi.org/10.1016/j.earscirev.2006.05.002.

Schobben, M., Heuer, F., Tietje, M., Ghaderi, A., Korn, D., Korte, C., Wignall, P.B., 2019. Chemostratigraphy across the Permian-Triassic boundary: the effect of sampling strategies on carbonate carbon isotope stratigraphic markers. In: Sial, A.N. (Ed.), Chemostratigraphy across Major Chronological Boundaries. Geophy. Mono. 240. pp. 159–181.

Sephton, M.A., Looy, C.V., Brinkhuis, H., Wignall, P.B., de Leeuw, J.W., Visscher, H., 2005. Catastrophic soil erosion during the end-Permian biotic crisis. Geology 33, 941–944. https://doi.org/10.1130/G21784.1.

Shen, S.Z., Crowley, J.L., Wang, Y., Bowring, S.A., Erwin, D.H., Sadler, P.M., Cao, C.Q., Rothman, D.H., Henderson, C.M., Ramezani, J., Zhang, H., Shen, Y., Wang, X.D., Wang, W., Mu, L., Li, W.Z., Tang, Y.G., Liu, X.L., Liu, L.J., Zeng, Y., Jiang, Y.F., Jin, Y.G., 2011. Calibrating the end-Permian mass extinction. Science 334, 1367–1372. https://doi.org/10.1126/science.1213454.

Shu, W.C., Tong, J.N., Tian, L., Benton, M.J., Chu, D.L., Yu, J.X., Guo, W.W., 2018. Limulid trackways from Permian-Triassic continental successions of North China. Palaeogeogr. Palaeoclimatol. Palaeoecol. 508, 71–90. https://doi.org/10.1016/j.palaeo.2018.07.022.

Smith, R.M.H., Botha-Brink, J., 2014. Anatomy of a mass extinction: Sedimentological and taphonomic evidence for a drought-induced die-offs at the Permian-Triassic boundary in the main Karoo Bason, South Africa. Palaeogeogr. Palaeoclimatol. Palaeoecol. 396, 99–118. https://doi.org/10.1016/j.palaeo.2014.01.002.

Song, H.J., Wignall, P.B., Tong, J.N., Yin, H.F., 2013. Two pulses of extinction during the Permian-Triassic crisis. Nat. Geosci. 6. https://doi.org/10.1038/NGEO1649.

Song, H.J., Wignall, P.B., Chu, D.L., Tong, J.N., Sun, Y.D., Song, H.Y., He, W.H., Tian, L., 2014. Anoxia/high temperature double whammy during the Permian-Triassic marine crisis and its aftermath. Sci. Rep. 4, 4132. https://doi.org/10.1038/srep04132.

Song, T., Tong, J.N., Tian, L., Chu, D.L., Huang, Y.F., 2019. Taxonomic and ecological variations of Permian/Triassic transitional bivalve communities from the littoral clastic facies in southwestern China. Palaeogeogr. Palaeoclimatol. Palaeoecol. 519, 108–123. https://doi.org/10.1016/j.palaeo.2018.02.027.

Stanley, S.M., 2016. Estimates of the magnitude of major marine mass extinctions in earth history. Proc. Natl. Acad. Sci. 113, E6325–E6334. https://doi.org/10.1073/pnas.1613094113.

Sun, Y.D., Joachimski, M.M., Wignall, P.B., Yan, C.B., Chen, Y.L., Jiang, H.S., Wang, L.N., Lai, X.L., 2012. Lethally hot temperatures during the early Triassic greenhouse. Science 388, 366–370. https://doi.org/10.1126/science.1224126.

Sun, H., Xiao, Y.L., Gao, Y.J., Zhang, G.J., Casey, J.F., Shen, Y.N., 2018. Rapid enhancement of chemical weathering recorded by extremely light seawater lithium isotopes at the Permian-Triassic boundary. Proc. Natl. Acad. Sci. 115, 3782–3787. https://doi.org/10.1073/pnas.1711862115.

Tang, H., Kershaw, S., Liu, H., Tan, X.C., Li, F., Hu, G., Huang, C., Wang, L.C., Lian, C.B., Li, L., Yang, X.F., 2017. Permian-Triassic boundary microbialites (PTBMs) in Southwest China: implications for paleoenvironment reconstruction. Facies 63, 2. https://doi.org/10.1007/s10347-016-0482-8.

Vajda, V., McLoughlin, S., Mays, C., Frank, T.D., Fielding, C.R., Tevyaw, A., Lehsten, V., Bocking, M., Nicoll, R.S., 2020. End-Permian (25Mya) deforestation, wildfires and flooding – An ancient biotic crisis with lessons for the present. Earth Planet. Sci. Lett. 529. https://doi.org/10.1016/j.epsl.2019.115875.

Wang, H., Shao, L., Hao, L.M., Zhang, P.F., Glasspool, I.J., Wheeley, J.R., Wignall, P.B., Yi, T.S., Zhang, M.Q., Hilton, J., 2011. Sedimentology and sequence stratigraphy of the Lopingian (late Permian) coal measures in southwestern China. Int. J. Coal Geol. 85, 168–183. https://doi.org/10.1016/j.coal.2010.11.003.

Wang, L.N., Wignall, P.B., Wang, Y.B., Jiang, H.S., Sun, Y.D., Li, G.S., Yuan, J.L., Lai, X.L., 2016. Depositional conditions and revised age of the Permo-Triassic microbialites at Gaohua section, Cili County (Hunan Province, South China). Palaeogeogr. Palaeoclimatol. Palaeoecol. 443, 156–166. https://doi.org/10.1016/j.palaeo.2015.11.032.

Ward, P.D., Montgomery, D.R., Smith, R., 2000. Altered river morphology in South Africa related to the Permian-Triassic extinction. Science 289, 1740–1743. https://doi.org/10.1126/science.289.5485.1740.

Wignall, P.B., 2015. The Worst of Times: How Life on Earth Survived 80 Million Years of Extinction. Princeton University Press, pp. 224.

Wignall, P.B., Hallam, A., 1992. Anoxia as a cause of the Permian/Triassic extinction: facies evidence from northern Italy and the western United States. Palaeogeogr.

Palaeoclimatol. Palaeoecol. 93, 21–46. https://doi.org/10.1016/0031-0182(92)90182-5.

Wignall, P.B., Kershaw, S., Collin, P.Y., Crasquin-Soleau, S., 2009. Erosional truncation of uppermost Permian shallow-marine carbonates and implications for Permian-Triassic boundary events: comment. Bull. Geol. Soc. Am. 121, 954–956. https://doi.org/10.1130/B26424.1.

Wu, Y.Y., Tong, J.N., Algeo, T.J., Chu, D.L., Cui, Y., Song, H.Y., Shu, W.C., Du, Y., 2020. Organic carbon isotopes in terrestrial Permian-Triassic boundary sections of North China: implications for global carbon cycle perturbations. Bull. Geol. Soc. Am. https://doi.org/10.1130/B35228.1.

Xie, S.C., Pancost, R.D., Huang, J.H., Wignall, P.B., Yu, J.X., Tang, X.Y., Chen, L., Huang, X.Y., Lai, X.L., 2007. Changes in the global carbon cycle occurred as two episodes during the Permian-Triassic crisis. Geology 35, 1083–1086. https://doi.org/10.1130/G24224A.1.

Yan, Z.M., Shao, L., Glasspool, I.J., Wang, J., Wang, X.T., Wang, H., 2019. Frequent and intense fires in the final coals of the Palaeozoic indicate elevated atmospheric oxygen levels at the onset of the end-Permian mass extinction event. Int. J. Coal Geol. 207, 75–83. https://doi.org/10.1016/j.coal.2019.03.016.

Yin, H.-F., Feng, Q.-L., Lai, X.-L., Baud, A., Tong, J.-N., 2007. The protracted Permo-Triassic crisis and multi-episode extinction around the Permian-Triassic boundary. Glob. Planet. Chang. 55, 1–20. https://doi.org/10.1016/j.gloplacha.2006.06.005.

Yin, H.F., Jiang, H.S., Xia, W.C., Feng, Q.L., Zhang, N., Shen, J., 2014. The end-Permian regression in South China and its implication on mass extinction. Earth-Sci. Rev. 137,

19–33. https://doi.org/10.1016/j.earscirev.2013.06.003.

Yu, J.X., Peng, Y.Q., Zhang, S.X., Yang, F.Q., Zhao, Q.M., Huang, Q.S., 2007. Terrestrial events across the Permian – Triassic boundary along the Yunnan-Guizhou border, SW China. Glob. Planet. Chang. 55, 193–208. https://doi.org/10.1016/j.gloplacha.2006.06.013.

Zhang, Y., Zhang, K.X., Shi, G.R., He, W.H., Yuan, D.X., Yue, M.L., Yang, T.L., 2014. Restudy of conodont biostratigraphy of the Permian-Triassic boundary section in Zhongzhai, southwestern Guizhou Province, South China. J. Asian Earth Sci. 80, 75–83. https://doi.org/10.1016/j.jseaes.2013.10.032.

Zhang, H., Cao, C.Q., Liu, X.L., Mu, L., Zheng, Q.F., Xiang, L., Liu, L.J., Shen, S.Z., 2016. The terrestrial end-Permian mass extinction in South China. Palaeogeogr. Palaeoclimatol. Palaeoecol. 448, 108–124. https://doi.org/10.1016/j.palaeo.2015.07.002.

Zhang, L.J., Buatois, L.A., Mángano, M.G., Qi, Y.-A., Zhang, X., Sun, S.-Q., Tai, C., 2017. Early Triassic estuarine depauperate *Cruziana* ichnofacies from the Sichuan area of South China and its implications for the biotic recovery in brackish-water settings after the end-Permian mass extinction. Palaeogeogr. Palaeoclimatol. Palaeoecol. 485, 351–360. https://doi.org/10.1016/j.palaeo.2017.06.025.

Zhu, Z.C., Liu, Y.Q., Kuang, H.W., Benton, M.J., Newell, A.J., Xu, H., An, W., Ji, S., Xu, S.C., Peng, N., Zhai, Q.G., 2019. Altered fluvial patterns in North China indicate rapid climate change linked to the Permian-Triassic mass extinction. Sci. Rep. 9, 16818. https://doi.org/10.1038/s41598-019-53321-z.